Video Article

A Modular Microfluidic Technology for Systematic Studies of Colloidal Semiconductor Nanocrystals

Robert W Epps[1], Kobi C Felton[1], Connor W Coley[2], Milad Abolhasani[1]

[1]Chemical and Biomolecular Engineering, North Carolina State University

[2]Chemical Engineering, Massachusetts Institute of Technology

Correspondence to: Milad Abolhasani at abolhasani@ncsu.edu

URL: https://www.jove.com/video/57666
DOI: doi:10.3791/57666

Keywords: Engineering, Issue 135, Microfluidics, high-throughput, modularity, micro-reaction engineering, perovskite, colloidal nanocrystals, quantum dots

Date Published: 5/10/2018

Citation: Epps, R.W., Felton, K.C., Coley, C.W., Abolhasani, M. A Modular Microfluidic Technology for Systematic Studies of Colloidal Semiconductor Nanocrystals. *J. Vis. Exp.* (135), e57666, doi:10.3791/57666 (2018).

Abstract

Colloidal semiconductor nanocrystals, known as quantum dots (QDs), are a rapidly growing class of materials in commercial electronics, such as light emitting diodes (LEDs) and photovoltaics (PVs). Among this material group, inorganic/organic perovskites have demonstrated significant improvement and potential towards high-efficiency, low-cost PV fabrication due to their high charge carrier mobilities and lifetimes. Despite the opportunities for perovskite QDs in large-scale PV and LED applications, the lack of fundamental and comprehensive understanding of their growth pathways has inhibited their adaptation within continuous nanomanufacturing strategies. Traditional flask-based screening approaches are generally expensive, labor-intensive, and imprecise for effectively characterizing the broad parameter space and synthesis variety relevant to colloidal QD reactions. In this work, a fully autonomous microfluidic platform is developed to systematically study the large parameter space associated with the colloidal synthesis of nanocrystals in a continuous flow format. Through the application of a novel translating three-port flow cell and modular reactor extension units, the system may rapidly collect fluorescence and absorption spectra across reactor lengths ranging 3 - 196 cm. The adjustable reactor length not only decouples the residence time from the velocity-dependent mass transfer, it also substantially improves the sampling rates and chemical consumption due to the characterization of 40 unique spectra within a single equilibrated system. Sample rates may reach up to 30,000 unique spectra per day, and the conditions cover 4 orders of magnitude in residence times ranging 100 ms - 17 min. Further applications of this system would substantially improve the rate and precision of the material discovery and screening in future studies. Detailed within this report are the system materials and assembly protocols with a general description of the automated sampling software and offline data processing.

Video Link

The video component of this article can be found at https://www.jove.com/video/57666/

Introduction

The advent of semiconductor nanocrystals, particularly quantum dots, has driven significant advancements in electronic materials research and manufacturing. For example, quantum dot LEDs[1] have already been implemented in commercially available "QLED" displays. More recently among this class of semiconductors, perovskites have sparked substantial interest and research towards high-efficiency and low-cost PV technologies. Since the first demonstration of a perovskite-based PV in 2009,[2] the lab-scale power conversion efficiency of perovskite-based solar cells has increased at a rate unparalleled by any PV technology in history.[3,4] In addition to the driving interest in perovskite-based PVs, a variety of recent methods describing the facile colloidal synthesis of perovskite nanocrystals have created the opportunity for low-cost, solution-phase processing of perovskite QDs in commercial electronics.[5,6,7,8,9,10,11,12,13,14]

In the effort towards large-scale nanomanufacturing of colloidal perovskite QDs, a better fundamental understanding of the nanocrystal growth pathways and an effective control of the reaction conditions must first be developed. However, existing studies of these processes have traditionally relied on flask-based approaches. Batch synthesis strategies present a variety of inherent limitations in terms of material characterization and production, but most significantly, flask-based techniques are highly inefficient in screening time and precursor consumption, and demonstrate flask size-dependent mass transfer properties, which inhibit the synthesis consistency.[15] To effectively study the growth pathways of colloidal semiconductor nanocrystals across the large variety of reported syntheses procedures and within the broad relevant sample space, a more efficient screening technique is required. Over the past two decades, a range of microfluidic strategies have been developed for studies of colloidal nanocrystals leveraging the substantially lower chemical consumption, the accessibility of high-throughput screening methods, and the potential for a process control implementation in continuous synthesis systems.[12,16,17,18,19,20]

In this work, we report the design and development of an automated microfluidic platform for the high-throughput *in situ* studies of colloidal semiconductor nanocrystals. A novel translating flow cell, a highly modular design, and the integration of off-the-shelf tubular reactors and fluidic connections form a unique and adaptable reconfigurable platform with direct applications in the discovery, screening, and optimization of colloidal nanocrystals. Capitalizing on the translational capability of our detection technique (*i.e.*, a three-port flow cell), for the first time, we demonstrate

the systematic decoupling of mixing and reaction timescales, while simultaneously improving the sampling efficiency and collection rates over traditional stationary flow cell approaches. The utilization of this platform enables the high-throughput and precise band-gap engineering of colloidal nanocrystal syntheses towards continuous nanomanufacturing strategies.

Protocol

1. Reactor Assembly

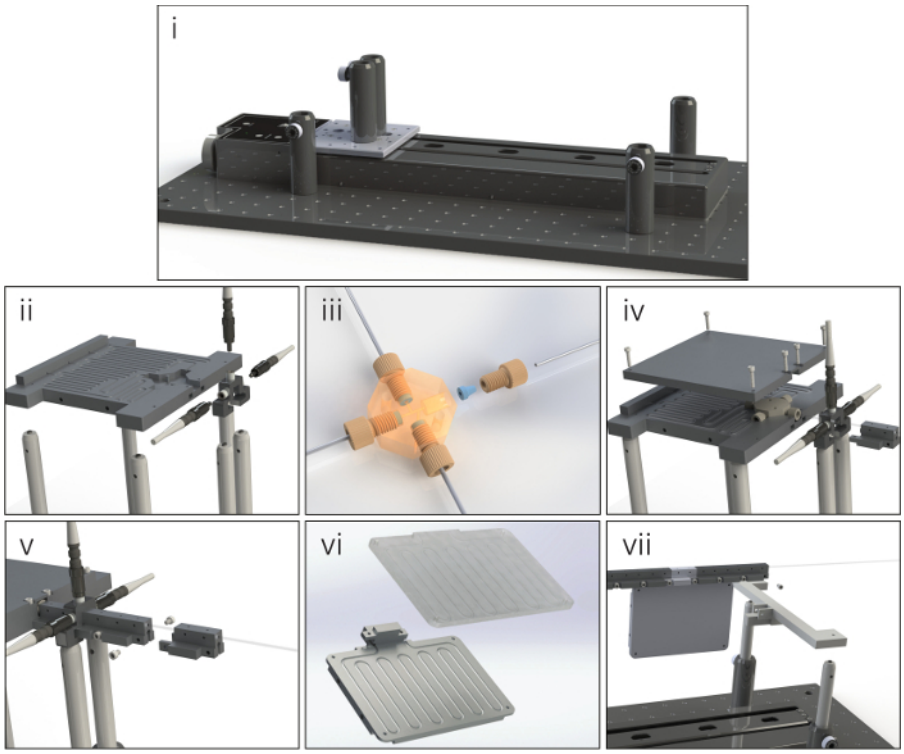

Figure 1. Step-by-step illustration of a sample platform assembly process. The panels shows a step-by-step illustration of a sample platform assembly process detailing (i) the initial arrangement of the translation stage and optical post holders on the mounting bread broad, (ii) the mounting of the precursor tube mounting stage and the flow cell onto optical posts, (iii) the attachment of the microfluidic tubing to the custom cross-junction which is under transparency to reveal flow pathways, (iv) the securing of the precursor tubing while simultaneously positioning the first sampling unit, (v) the subsequent connection of additional sampling units with the reactor tubing run through each module, (vi) the tubing pathway of the reactor extension units, and (vii) the securing of the final sampling unit to support the structure and optical posts. Please click here to view a larger version of this figure.

Note: Due to the wide array of possible configurations, the exact assembly process of the microfluidic platform might vary; however, the general methods are the same for all arrangements. Detailed below and in **Figure 1** is the platform assembly process for a two-precursor, multi-phase flow format with a single extension unit after the 14th sampling port.

1. Secure the translation stage and post holders to the optical breadboard. Connect the junction mounting stage and flow cell to the posts and fasten them to the platform.
2. Wire the reactor tubing and precursor feed lines to the custom cross-junction and feed the tubing through the channels in the raised stage. Ensure that each tubing segment is cut to a length that may comfortably reach the respective syringe pump or collection vial.
3. Connect the first sampling port unit to the junction stage and fasten the precursor line cover to the raised mounting stage, securing all the tubular components and the first sampling unit in place.
4. Add additional modular reactor units by running the reactor tubing through the desired component and connecting the segments to the rest of the assembled structure. Build out the units from the junction until the desired length and arrangement is obtained.
   NOTE: The reactor tubing should fit firmly within each unit. Deformations in the tubing (stretching, crimping, etc.) significantly affect the optical signal strength.
5. Fasten the support structure to the outlet of the last sampling segment and secure the support to the optical posts connected to the breadboard.
6. Connect the feed lines of the flow system to the computer-controlled syringe pumps and feed the reactor outlet into a nitrogen gas pressurized (~12 psig) collection vial.
7. Connect 3 fiber optic patch cords to the 3 flow cell ports, and attach the opposite ends to the spectrometer, LED, and deuterium-halogen (DH) light source respectively. Ensure that the cables are able to move smoothly with the full length of the translation stage and without any unnecessary strain on their connection with the flow cell to complete platform assembly (as shown in **Figure 2**).

2. Precursor Preparation

NOTE: The reaction screening system may be applied to the synthesis of various colloidal semiconductor nanocrystals; however, for the purpose of platform development and validation, a $CsPbBr_3$ perovskite synthesis, adapted from Wei *et al.*[6] to better suit flow analyses, was used as a case study reaction. The precursor preparation process is detailed below.

1. Prepare 15 mL of 0.013 M bromide precursor by combining 109 mg of tetraoctylammonium bromide, 1 mL of oleic acid, and 14 mL of toluene in a sealed 20-mL vial.
2. Stir the mixture vigorously at room temperature until a clear solution is obtained.
3. Prepare 48 mL of 0.0021 M cesium-lead precursor by first combining 0.6 mmol of cesium hydroxide, 0.6 mmol of lead(II) oxide, and 3 mL of oleic acid in a sealed 8-mL vial with a septum.
    1. Pierce the septum with a needle for ventilation and heat the solution at 160 °C in an oil bath and vigorously stir it until a clear solution forms (approximately 15 minutes).
    2. Move the vial and needle to an oven and heat them at 120 °C for 1 h, then remove the venting needle and allow the solution to cool to room temperature in open air.
4. Add 0.5 mL of the high concentration cesium-lead mixture to 47.5 mL of toluene in a sealed 50-mL vial and stir vigorously.
5. Load the bromide precursor and dilute the cesium-lead precursor into their respective syringes and begin the automated characterization process by flowing the two precursors together at the desired conditions (see step 3).
   NOTE: For the experiments detailed under **Representative Results**, volumetric injection ratios of 6.4:1 of cesium-lead to bromide and 1:1 of gas carrier phase to net liquid were used at variable total flow rates.

3. Interface Operation

Note: The entirety of the data collection is carried out through the automated reaction platform after the user specifies a series of flow conditions to be tested. The general procedures for operating the user interface during this initial input period are detailed below.

1. Open the automated operation software to view the user interface front panel (shown in **Figure 3**).
2. Move to the **Spectrometer settings** panel and begin filling all inputs.
    1. Paste the file path for the desired data saving folder in the **File root for data** box.
    2. Under **Spectrometer VISA**, select the USB connection address for the spectrometer. If the spectrometer USB address is not known, identify its location through the desktop's **Device Manager** page.
    3. Select the **integration time**, the **number of spectra to average per sample**, and the **number of spectra to save per condition** for both absorption **(Abs)** and fluorescence (Flu). In the case of the synthesis detailed in step 2, set an integration time of 12 ms for the absorption and 4 ms for the fluorescence averaged over 10 spectra.
    4. If characterizing single-phase flow, move on to the next step, leaving the **Multiphase** button off. If characterizing multi-phase flow, select the **Multiphase** button and set the **minimum sample length** so that approximately 2 complete gas-liquid oscillations may pass the sampling point. Then assign the **number of samples** to take within that sampling window.
       NOTE: The sampling time-resolution within a multi-phase flow may be limited by the spectrometer settings, and adjustments may be needed if seeking a higher resolution.
3. Move to the **Pump configuration** panel and begin filling all inputs.
    1. Under **Syringe 1 COM, Syringe 2 COM,** and **Dual Pump COM,** assign USB communication addresses to all pumps. See step 3.2.2 for the address identification process.
    2. Set the **syringe inner diameters**, which may be found on the pump interface or within the syringe manuals, for all syringes in use. For configurations not implementing all syringes, leave the extraneous syringe diameters at the default values.
    3. If collecting absorption reference spectra, identify an acceptable blank solution, load it into an attached syringe, and set the respective syringe to a moderate flow rate (approximately 300 µL/min) in the respective **Ref flow rate** box.
4. Move to the **System configuration** panel and begin filling all inputs.
    1. If the stage locations have been optimized and are properly displayed under **Stage positions**, select the **Use previous position** button and move to the next step. If the stage locations have not been optimized, assign a stage position window size and link the approximate stage positions (within the position range) using a .csv vector and the **File path** box. Leave the **Stage increment** box at 0.5 mm and the **Startup Passes** box at 8.
    2. Calculate the volume of the reactor segment from the center of the junction to the final sampling port and input that value into the **System volume** box. Leave the **Minimum equilibrium time** at 10 s.
5. Double-check the accuracy of all inputs and select the **Run** button in the top left of the interface.
   NOTE: Inputs on the front panel may not be changed once the software has begun its operation.
6. In the **Save reference spectra** window, select **Yes** if the reference spectra will be saved or **No** if they will not.
7. In the **Set condition flow rates** window, select up to 30 desired flow rate configurations to test, leaving all unused syringe inputs blank.
8. Select **OK** and allow the system to run until all desired conditions have been sampled; the system shuts down on its own. If the system needs to be stopped for any reason, select the **Stop early** button and allow the process to shut down.
   CAUTION: Using the **Abort** button on the top left of the interface will not allow the system to shut down pumps or light sources, potentially damaging equipment and/or posing a significant health risk via UV light exposure.

4. Pathlength Corrections

1. To obtain the pathlength correction correlation for each port, first inject a stable solution of perovskites dispersed in toluene into the reactor segment until the reactor tubing is uniformly filled.
2. Run the automated sampling process on this uniform solution for 4 full passes of the flow cell (see step 3 for the operation procedure).
3. Apply baseline corrections for both fluorescence and absorption spectra, then average overall for the passes by port location. Normalize all curves in reference to the wavelength intensities at 455 nm and 485 nm for absorption and fluorescence respectively (see **Figure 4**).
4. Use the normalization factor calculated at each port to proportionally scale the curves of all subsequent spectra.

Representative Results

Sample spectra: Utilizing the discussed microfluidic platform, the nucleation and growth stages of colloidal semiconductor nanocrystals at the synthesis temperature can be directly studied by monitoring the time-evolution of the absorption and fluorescence spectra of the formed nanocrystals under uniform mixing conditions. **Figure 5A** shows an example set of spectra obtained within a single pass of the three-port flow cell. While the emission wavelength distributions alone provide valuable insight towards applications in high-quality LED manufacturing, fitting the absorption and emission bandgap energies within experimentally validated Effective Mass Approximation models would enable the continuous monitoring of nanoparticle size distributions throughout the syntheses.[14] Equivalent sets of spectra were obtained at varying flow rates and reactor lengths, which allowed for a data collection across residence times spanning 100 ms - 17 min.

Kinetically tunable nanocrystals: The axisymmetric recirculation patterns formed within the liquid segments of multi-phase flow enables velocity-dependent mass transfer control.[21] A study of the velocity-dependent mixing timescale to residence time demonstrated the kinetic tunability in nanocrystal growth pathways for the perovskite QDs (see **Figure 5B**). Our developed modular platform allows, for the first time, a systematic study of the effect of early-stage mixing time on the final optical properties of formed nanocrystals. Through variations in the reactive slug velocity, while maintaining all other parameters constant, a difference in peak emission wavelengths as great as 25 nm at an equivalent residence time was observed. Further evaluations of the colloidal system illustrated that the observed difference in emission wavelength was maintained at longer residence times, resulting in stable, kinetically tunable nanocrystals.[15]

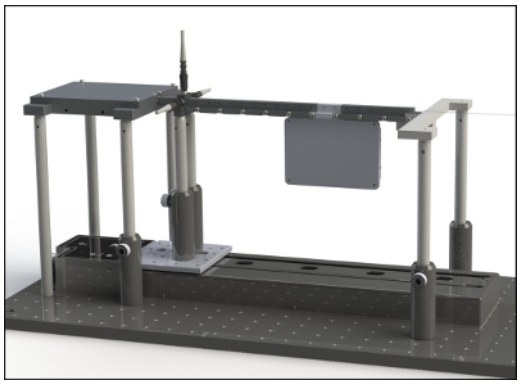

Figure 2. Fully assembled automated reaction screening platform. This figure shows a fully assembled automated reaction screening platform with a single reactor extension unit between the 14th and 15th sampling port. Please click here to view a larger version of this figure.

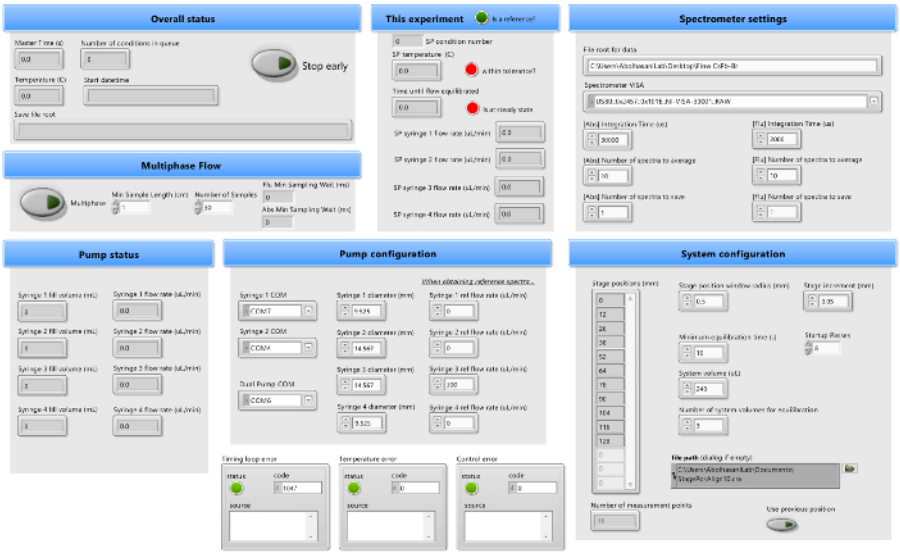

Figure 3. User interface for automated platform operation. This panel shows the user interface, which allows for the control and tuning of parameters such as the syringe flow rates, spectrometer measurement conditions, and sampling position, for the characterization across a broad range of colloidal semiconductor nanocrystal syntheses. Please click here to view a larger version of this figure.

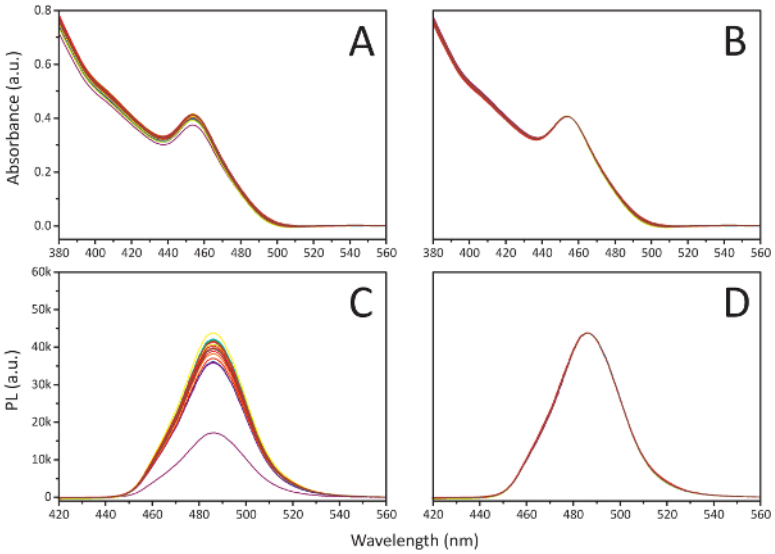

Figure 4. Process for pathlength correction. This panel shows the process for a pathlength correction by port using **A**. absorption spectra collected over 20 sampling ports with **B**. the spectra normalized with respect to the absorbance at 455 nm on a solution of colloidal $CsPbBr_3$ perovskites dispersed in toluene and **C**. respective photoluminescence (PL) spectra **D**. normalized to the 485 nm signal intensity. Adapted from Epps *et al.*[15] with permission of The Royal Society of Chemistry. Please click here to view a larger version of this figure.

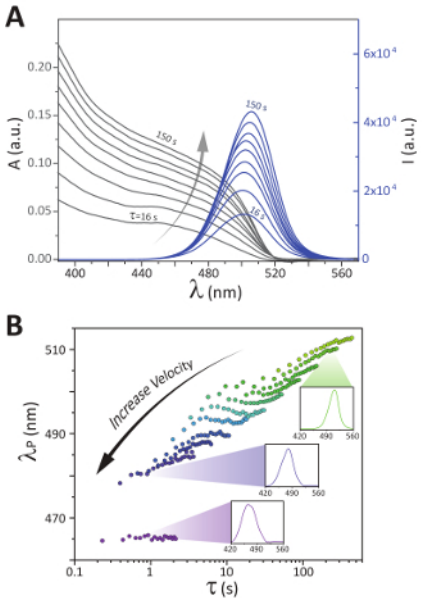

Figure 5.**Sample spectra and demonstration of kinetic tunability**. These panels show **A**. the absorption (A) and fluorescence (I) spectra collected within a single pass of the flow cell on a multiphase, reactive $CsPbBr_3$ perovskite system moving at an average slug velocity of approximately 0.2 cm/s, and **B**. the peak fluorescence wavelength (λ_P) as a function of the residence time plotted for 11 different average slug velocities ranging from 0.6 to 130 mm/s with sample fluorescence spectra shown at residence times and slugs velocities of 200 s and 1.0 mm/s (top), 0.9 s and 75 mm/s (middle), and 0.9 s and 130 mm/s (bottom). Adapted from Epps *et al.*[15] with permission of The Royal Society of Chemistry. Please click here to view a larger version of this figure.

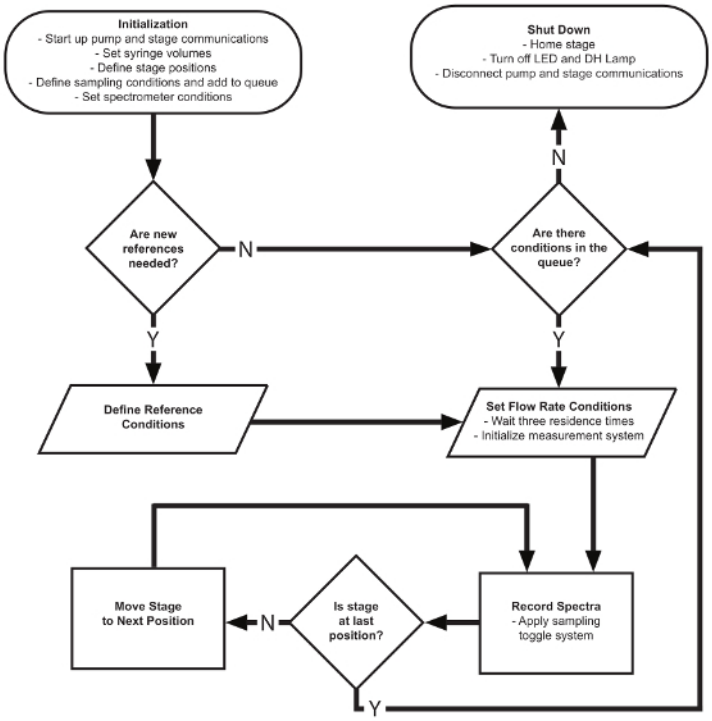

Figure 6. Process flow chart for the overall software-controlled data collection process. This includes the initialization of the process hardware, the recursive sampling progressions, and the final shutdown of the platform. Adapted from Epps *et al.*[15] with permission of The Royal Society of Chemistry. Please click here to view a larger version of this figure.

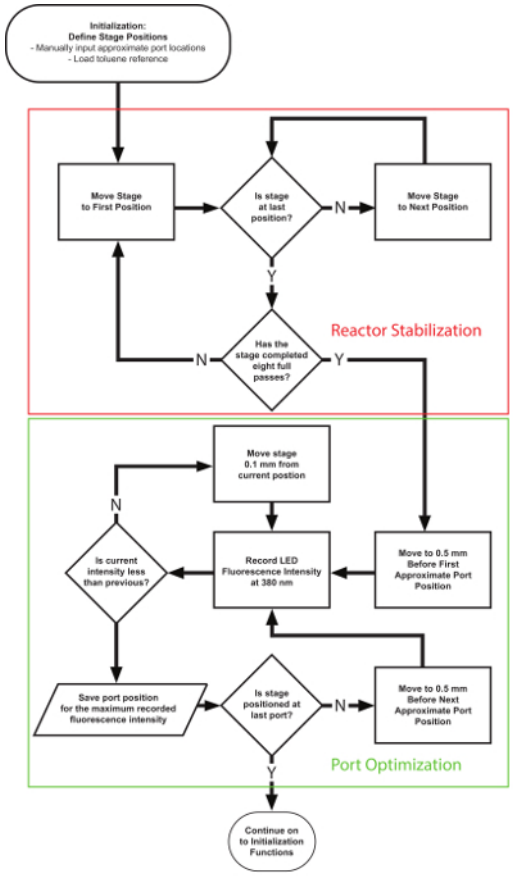

Figure 7. Automation software process flow chart for the port location assignment method. The algorithm first runs a specified number of stabilizing passes of the flow cell followed by an optimal port detection through the spectrometer reading of the LED signal intensity. Please click here to view a larger version of this figure.

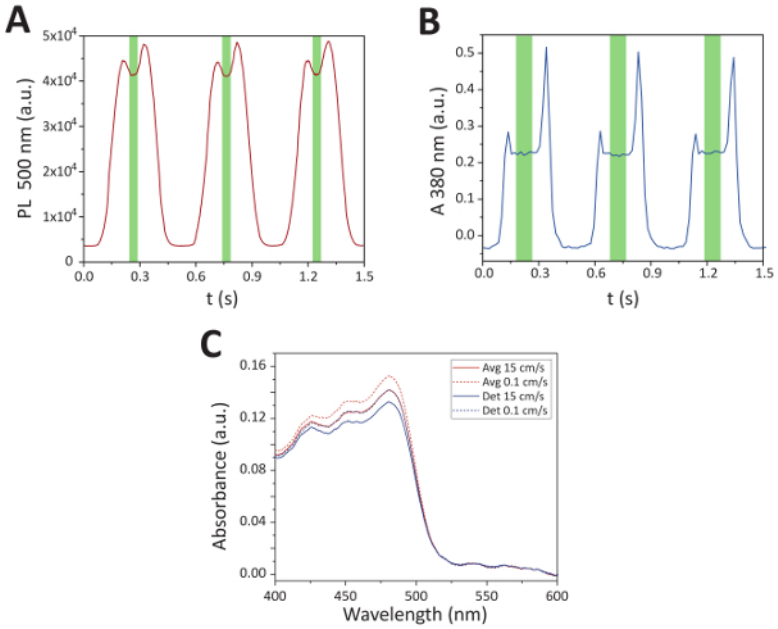

Figure 8. Sample multi-phase spectra isolation. These panels show the sample multi-phase spectra isolation for **A**. fluorescence at 500 nm and **B**. absorbance at 380 nm over time for a solution of perovskites dispersed in toluene. The green region indicates the range of ideal sampling times. Panel **C**. shows the absorption spectra (fluorescein solution) comparing multi-phase sampling methods as it relates to the slug velocity. "Det" indicates that the plug detection algorithm was applied, and "Avg" indicates that samples were taken over even intervals of time and averaged together. Note that the plug detection method applied to slower moving slugs produced equivalent spectra as the simple average of the higher velocity system. Adapted from Epps *et al.*[15] with permission of The Royal Society of Chemistry. Please click here to view a larger version of this figure.

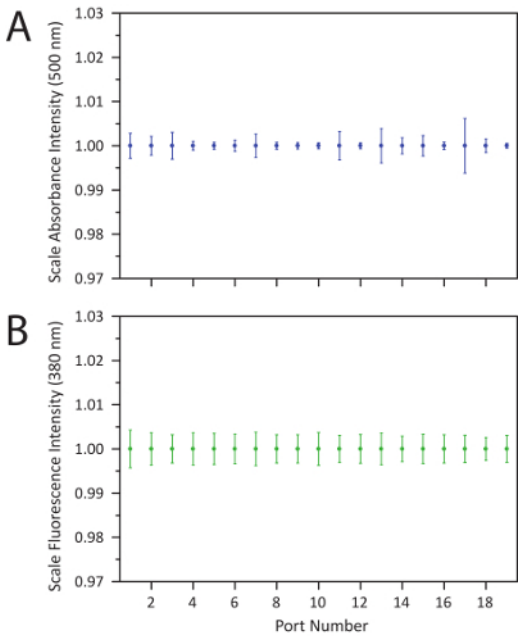

Figure 9. Demonstration of measurement stability across stage passes. This is a demonstration of the measurement stability across stage passes using **A**. the absorption signal intensity at 500 nm and **B**. the fluorescence intensity at 380 nm on a toluene reference normalized by port location and averaged over 30 full passes of the flow cell. The error bars indicate a 95% confidence interval, and no values deviated beyond ± 1% of the average reading. Adapted from Epps *et al.*[15] with permission of The Royal Society of Chemistry. Please click here to view a larger version of this figure.

Discussion

Automated sampling system: The autonomous operation of the screening platform is carried out with a central control finite state machine. Movement between these states occurs sequentially with multiple recursive segments to allow for operation across a varying number of sampling conditions. The general system controls can be divided into 3 core stages. First, the system begins with an initialization step, which establishes communications through each USB-controlled component, automatically defines file saving pathways, and prompts for initial user inputs. The program then runs through the sampling process for every entered reaction condition until all the desired data has been collected. Finally, a termination process returns all hardware to the starting position before ending the script operation. The general movement within this software is detailed in **Figure 6**.

Port detection: Within the main automation framework are several critical subfunctions that enable effective and efficient reaction characterizations. First, **Figure 7** shows a portion of the "Initialization" segment where the sampling port positions are defined for the translation stage. The port detection function first stabilizes the reactor segment by mimicking flow cell movement along the reactor for 8 full passes.It then detects the optimal port location by sampling the fluorescence intensity across a 1-mm window around the estimated location and selecting the position of the maximum intensity.This location is saved for each port and used as the stage positions during subsequent sampling procedures.

Light source toggling: The efficient absorbance and fluorescence spectra sampling within the three-port flow cell is carried out with an automated light source toggling system. Upon reaching the sampling port, 10 spectra for both absorbance at a 15-ms integration time and fluorescence at a 4-ms integration time may be collected in as little as 400 ms. When moving between sample locations, both the DH Lamp and LED are toggled off. Upon reaching the desired sampling port, the DH Lamp is triggered on, and the absorbance sampling conditions are set on the spectrometer, followed by sample collection. The DH Lamp is then toggled off, while the LED is toggled on. The sampling process is repeated for the fluorescence conditions, and both lights are then turned off.

Slug detection: In multi-phase flow systems, efficient sample collection requires a combination of sampling techniques, which depend upon the velocity of the moving slug. The threshold slug velocity where a detection algorithm becomes less effective than simple averaging was found to occur at approximately 11 mm/s. In the case of lower velocity systems, single spectra sampling is carried out at uniform intervals across the estimated length of 2 fluid slugs (approximately 1 cm). Within the spectra obtained through this sampling process, the 10 optimal spectra in the bulk fluid center of the slug are isolated using a five-point local variance of a given wavelength over time - 400 nm for fluorescence and 380 nm for absorbance - as shown in **Figure 8**. Within higher fluid velocity systems, however, the available sampling window of a single moving slug surpasses the effective sampling rate of the spectrometer. In these instances, averaging together 10 spectra collected over uniform intervals was found to be sufficient.

System specs: Through the application of multiple 87-cm extension units, sampling ports may be positioned at reactor tubing lengths varying 3 - 196 cm. The combination of varying flow rates and flow-cell movement enables *in situ* spectral characterization at residence times ranging 100 ms - 17 minutes with a sampling rate as high as 30,000 spectra per day. Furthermore, each absorption or fluorescence spectrum was obtained with notably low chemical consumption, requiring only 2 µL per spectra at the time of sampling and 20 µL per spectra overall (from startup to shutdown). This high sampling rate and efficiency can be attributed to the collection of up to 40 unique spectra within a single equilibrated system through the translating flow cell. After applying the reactor stabilization, port alignment, and pathlength correction processes, the platform was shown to be accurate for over 30 full passes of the flow cell (**Figure 9**). In a characterization of the respective light source signal intensities on a toluene reference, it was found that the error in counts of a given wavelength for each port remained within 1% across all 30 passes in both the fluorescence and absorption signals. This stability in the reactor measurement system enabled extensive material discovery, screening, and optimization studies to be carried out with minimal manual interference, resulting in more consistent data collection from the same batch of precursors.

Extended sampling space: The relationship between fluid velocity and residence time has often been confounded in existing synthesis screening studies. For characterizations implementing a stationary flow cell, for example, variable residence times are obtained by adjusting net fluid velocities. However, as detailed by the previously discussed evaluation of kinetic tunability in nanocrystal growth, this method of reaction characterization is likely insufficient for studies of a wide range of colloidal semiconductor syntheses with fast nucleation and growth kinetics. Decoupling the residence time from the fluid velocity by applying a portable sampling system expands the sampling space in a manner that has not been explored previously. Thus, the developed modular technology enables discovery and exploratory studies of the next generation of colloidal nanomaterials with significantly enhanced precision and control over the synthesis conditions.

Disclosures

North Carolina State University has filed a provisional patent (#62/558,155) on the discussed microfluidic platform.

Acknowledgements

The authors gratefully acknowledge the financial support provided by North Carolina State University. Milad Abolhasani and Robert W. Epps gratefully acknowledge financial support from the UNC Research Opportunities Initiative (UNC-ROI) grant.

References

1. Tan, Z.-K., Moghaddam, R. S. *et al.* Bright light-emitting diodes based on organometal halide perovskite. *Nature Nanotechnology.* **9** (9), 687-692 (2014).

2. Kojima, A., Teshima, K., Shirai, Y., Miyasaka, T. Organometal halide perovskites as visible-light sensitizers for photovoltaic cells. *Journal of the American Chemical Society.* **131** (17), 6050-6051 (2009).
3. Huang, H., Bodnarchuk, M. I., Kershaw, S. V, Kovalenko, M. V, Rogach, A. L. Lead halide perovskite nanocrystals in the research spotlight: stability and defect tolerance. *ACS Energy Letters.* **2** (9), 2071-2083 (2017).
4. Grätzel, M. The light and shade of perovskite solar cells. *Nature Materials.* **13**, 838 (2014).
5. Schmidt, L. C., Pertegás, A. *et al.* Nontemplate synthesis of CH3NH3PbBr3 perovskite nanoparticles. *Journal of the American Chemical Society.* **136** (3), 850-853 (2014).
6. Wei, S., Yang, Y., Kang, X., Wang, L., Huang, L., Pan, D. Room-temperature and gram-scale synthesis of CsPbX3 (X = Cl, Br, I) perovskite nanocrystals with 50-85% photoluminescence quantum yields. *Chemical Communications.* **52** (45), 7265-7268 (2016).
7. Vybornyi, O., Yakunin, S., V. Kovalenko, M. Polar-solvent-free colloidal synthesis of highly luminescent alkylammonium lead halide perovskite nanocrystals. *Nanoscale.* **8** (12), 6278-6283 (2016).
8. Sun, S., Yuan, D., Xu, Y., Wang, A., Deng, Z. Ligand-mediated synthesis of shape-controlled cesium lead halide perovskite nanocrystals via reprecipitation process at room temperature. *ACS Nano.* **10** (3), 3648-3657 (2016).
9. Jellicoe, T. C., Richter, J. M. *et al.* Synthesis and optical properties of lead-free cesium tin halide perovskite nanocrystals. *Journal of the American Chemical Society.* **138** (9), 2941-2944 (2016).
10. Tong, Y., Bladt, E. *et al.* Highly luminescent cesium lead halide perovskite nanocrystals with tunable composition and thickness by ultrasonication. *Angewandte Chemie International Edition.* **55** (44), 13887-13892 (2016).
11. Zhang, D., Eaton, S. W., Yu, Y., Dou, L., Yang, P. Solution-phase synthesis of cesium lead halide perovskite nanowires. *Journal of the American Chemical Society.* **137** (29), 9230-9233 (2015).
12. Lignos, I., Stavrakis, S., Nedelcu, G., Protesescu, L., deMello, A. J., Kovalenko, M. V. Synthesis of cesium lead halide perovskite nanocrystals in a droplet-based microfluidic platform: fast parametric space mapping. *Nano Letters.* **16** (3), 1869-1877 (2016).
13. Wei, S., Yang, Y., Kang, X., Wang, L., Huang, L., Pan, D. Room-temperature and gram-scale synthesis of CsPbX3 (X = Cl, Br, I) perovskite nanocrystals with 50-85% photoluminescence quantum yields. *Chemical Communications.* **52** (45), 7265-7268 (2016).
14. Protesescu, L., Yakunin, S. *et al.* Nanocrystals of cesium lead halide perovskites ($CsPbX_3$, X = Cl, Br, and I): novel optoelectronic materials showing bright emission with wide color gamut. *Nano Letters.* **15** (6), 3692-3696 (2015).
15. Epps, R. W., Felton, K. C., Coley, C. W., Abolhasani, M. Automated microfluidic platform for systematic studies of colloidal perovskite nanocrystals: towards continuous nano-manufacturing. *Lab Chip.* **23** (17), 4040-4047 (2017).
16. Lignos, I., Protesescu, L. *et al.* Facile droplet-based microfluidic synthesis of monodisperse IV-VI semiconductor nanocrystals with coupled in-line NIR fluorescence detection. *Chemistry of Materials.* **26** (9), 2975-2982 (2014).
17. Park, J. Il, Saffari, A., Kumar, S., Günther, A., Kumacheva, E. Microfluidic synthesis of polymer and inorganic particulate materials. *Annual Review of Materials Research.* **40** (1), 415-443 (2010).
18. Phillips, T. W., Lignos, I. G., Maceiczyk, R. M., deMello, A. J., deMello, J. C. Nanocrystal synthesis in microfluidic reactors: where next? *Lab on a Chip.* **14** (17), 3172-3180 (2014).
19. Lignos, I., Stavrakis, S., Kilaj, A., deMello, A. J. Millisecond-timescale monitoring of PBS nanoparticle nucleation and growth using droplet-based microfluidics. *Small.* **11** (32), 4009-4017 (2015).
20. Abolhasani, M., Coley, C. W., Xie, L., Chen, O., Bawendi, M. G., Jensen, K. F. Oscillatory microprocessor for growth and *in situ.* characterization of semiconductor nanocrystals. *Chemistry of Materials.* **27** (17), 6131-6138 (2015).
21. Chen, D. L., Gerdts, C. J., Ismagilov, R. F. Using microfluidics to observe the effect of mixing on nucleation of protein crystals. *Journal of the American Chemical Society.* **127** (27), 9672-9673 (2005).

